NANO LETTERS

Letter

pubs.acs.org/NanoLett

Evidence for Ultralow-Energy Vibrations in Large Organic Molecules

Hui Chen,[†,⊥] Thomas Pope,[‡,⊥] Zhuo-Yan Wu,[§,⊥] Dongfei Wang,[†,⊥] Lei Tao,[†] De-Liang Bao,[†] Wende Xiao,[†] Jun-Long Zhang,[§] Yu-Yang Zhang,[†,∥] Shixuan Du,[*,†] Song Gao,[§] Sokrates T. Pantelides,[∥,†] Werner A. Hofer,[*,‡] and Hong-Jun Gao[*,†]

[†]Institute of Physics & University of Chinese Academy of Sciences, Chinese Academy of Sciences, P.O. Box 603, Beijing 100190, China

[‡]School of Chemistry, Newcastle University, Newcastle upon Tyne NE1 7RU, United Kingdom

[§]Beijing National Laboratory for Molecular Sciences, State Key Laboratory of Rare Earth Materials Chemistry and Applications, College of Chemistry and Molecular Engineering, Peking University, Beijing 100871, China

[∥]Department of Physics and Astronomy and Department of Electrical Engineering and Computer Science, Vanderbilt University, Nashville, Tennessee 37235, United States

Supporting Information

ABSTRACT: The quantum efficiency or the rate of conversion of incident photon to free electron in photosynthesis is known to be extremely high. It has long been thought that the origin of this efficiency are molecular vibrations leading to a very fast separation of electrons and holes within the involved molecules. However, molecular vibrations are commonly in the range above 100 meV, which is too high for excitations in an ambient environment. Here, we analyze experimental spectra of single organic molecules on metal surfaces at ∼4 K, which often exhibit a pronounced dip. We show that measurements on iron(II) [tetra-(pentafluorophenyl)]porphyrin resolve this single dip at 4 K into a series of step-shaped inelastic excitations at 0.4 K. Via extensive spectral maps under applied magnetic fields and corresponding theoretical analysis we find that the dip is due to ultralow-energy vibrations of the molecular frame, typically in the range below 20 meV. The result indicates that ultralow energy vibrations in organic molecules are much more common than currently thought and may be all-pervasive for molecules above a certain size.

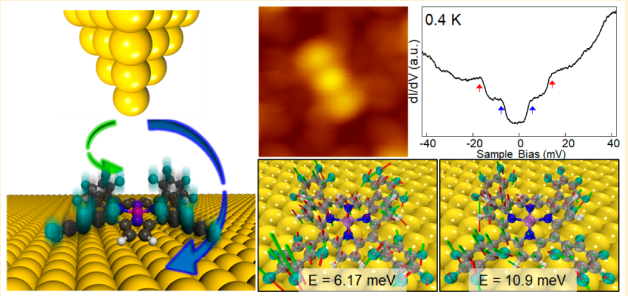

KEYWORDS: *Organic molecules, inelastic electron tunneling spectroscopy, ultralow-energy vibrations, Kondo resonance*

Photosynthesis, or the conversion of carbon dioxide and water to sugar with the help of sunlight, is arguably the basis of all life on Earth. A crucial step in the process is the creation of free electrons and holes, which can be used to drive reactions at different reaction centers. Although light, which elevates an electron into the conduction band, is necessary to drive the reaction, it is not in itself sufficient for a successful photosynthetic cycle, as the recombination probability would be in most cases too high.[1] However, a photosynthetic cycle would be possible only if vibrations are excited at low energy in a range substantially below 100 meV. To our knowledge, vibrations in this range, affecting not only single bonds but the whole molecular frame, have not been observed so far.[2]

Scanning tunneling microscopy and spectroscopy (STM/STS) at low temperature reveal a pronounced zero-bias dip in the differential conductance (dI/dV) spectra at ∼4.2 K for a variety of single organic molecules supported on metal surfaces.[3−11] The zero-bias dips are interpreted as Kondo antiresonances and the corresponding Kondo temperatures (T_k) are deduced to be on the order of 100 K, which is much higher than that of isolated magnetic atoms (T_k = 10−100 K).[12−15] However, the Kondo temperature $T_k \propto e^{-1/\rho J}$, where ρ and J are the density of states at Fermi level (E_F) of the metal substrate and the exchange coupling between the local spin and the substrate, respectively. As J in a molecular Kondo system is usually smaller than in an atomic Kondo system, one would expect a lower T_k in a molecular Kondo system, in contrast to previous experimental analysis.[3−11] The origin of this discrepancy has remained elusive.

Here, we demonstrate that the dip at the E_F in these systems most likely has a very different origin, which only becomes evident once the temperature in the experiments is lowered below 0.5 K. Moreover, it will be shown that even at this temperature range the interpretation of the experiments if far from clear-cut.

In our work, iron(II) [tetra-(pentafluorophenyl)]porphyrin molecules ($FeF_{20}TPP$, shown in Figure 1a) were synthesized on Au(111) through on-surface dechlorination reactions of $FeF_{20}TPPCl$[16] via thermal annealing at 400 K (for details see

Received: May 10, 2017
Revised: July 18, 2017
Published: July 20, 2017

DOI: 10.1021/acs.nanolett.7b01963
Nano Lett. 2017, 17, 4929−4933

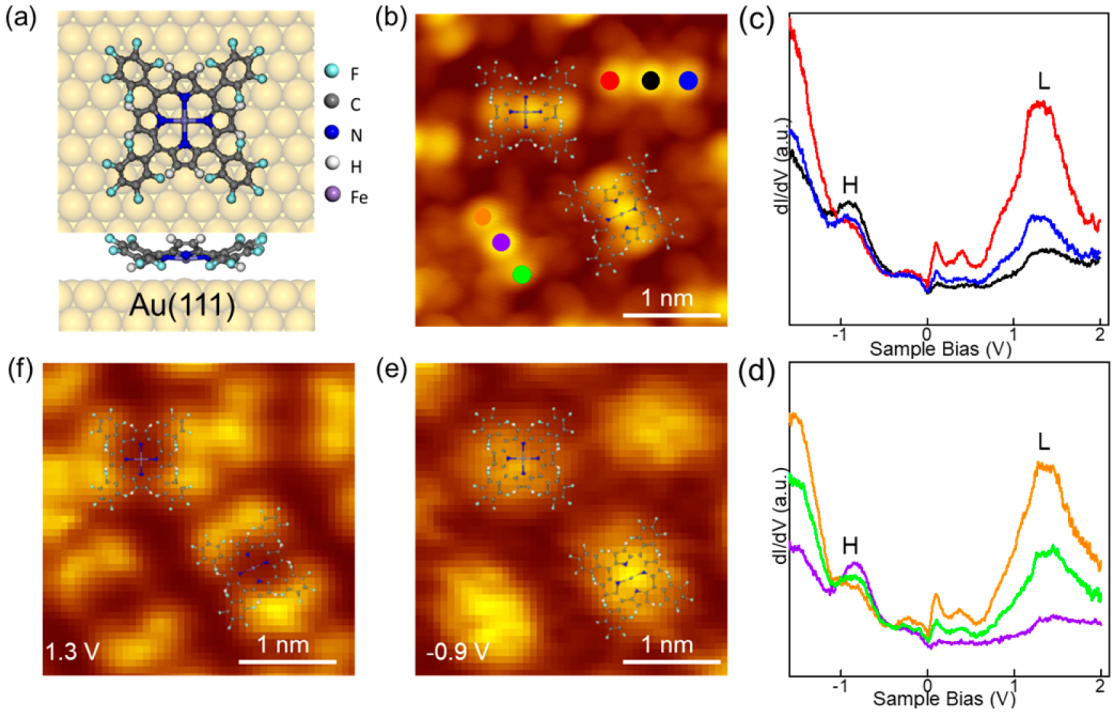

Figure 1. Configuration, STM images, and STS of $FeF_{20}TPP$ on Au(111). (a) Top (upper) and side (lower) views of the optimized configuration of $FeF_{20}TPP$ adsorbed on Au(111). (b) STM image showing the intramolecular structure of the $FeF_{20}TPP$ molecules. The structural models of $FeF_{20}TPP$ are overlaid on two of the molecules (sample bias, $U = -0.3$ V; tunneling current, $I = 0.1$ nA). (c,d) Site-specific dI/dV spectra ($U = -0.6$ V, $I = 0.1$ nA; lock-in modulation: $V_{rms} = 5$ mV) measured at the points (same color code) marked in (b). The HOMO and LUMO are indicated by "H" and "L", respectively. (e,f) dI/dV maps of $FeF_{20}TPP$ molecules taken from the same area of (b) at indicated bias voltages. dI/dV maps of $FeF_{20}TPP$ molecules taken from the same area of (b) at indicated bias voltages.

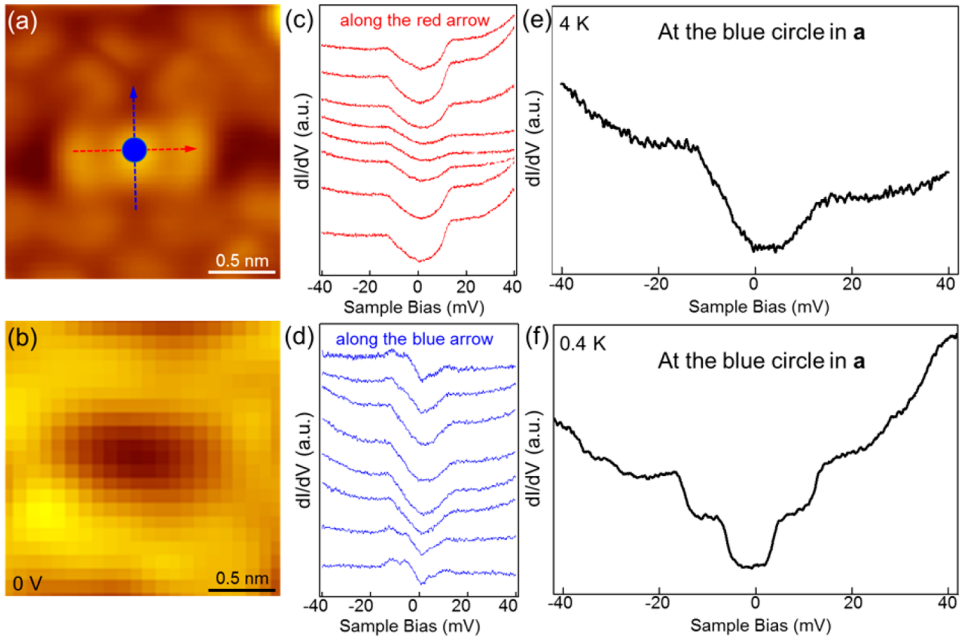

Figure 2. Kondo-like dip at 4.2 and 0.4 K. (a) STM topography ($U = -0.2$ V, $I = 0.1$ nA). (b) dI/dV map taken from the same area of (a) at 0 V showing the intramolecular distribution of the dip feature. (c,d) dI/dV spectra measured at a series of positions along the blue and red dashed lines indicated in (a) at 4 K, respectively ($U = -40$ mV, $I = 0.3$ nA; $V_{rms} = 0.5$ mV). (e,f) Comparison of dI/dV spectra taken at the central Fe^{2+} of $FeF_{20}TPP$/Au(111) at 4 K (e, $U = -40$ mV, $I = 0.3$ nA; $V_{rms} = 0.5$ mV) and 0.4 K (f, $U = -40$ mV, $I = 0.3$ nA; $V_{rms} = 0.5$ mV).

Supporting Information S1). The $FeF_{20}TPP$ molecules form ordered close-packed islands with a unit cell including two molecules with different azimuthal orientation (Figure 1b and Figure S1). Each molecule exhibits a saddle shaped conformation after adsorption on Au(111), as displayed in Figure 1a. The two upward pyrrole rings and the central Fe^{2+} ions give rise to the central rodlike protrusion with three maxima for each molecule in topographic STM images (Figure

DOI: 10.1021/acs.nanolett.7b01963
Nano Lett. 2017, 17, 4929−4933

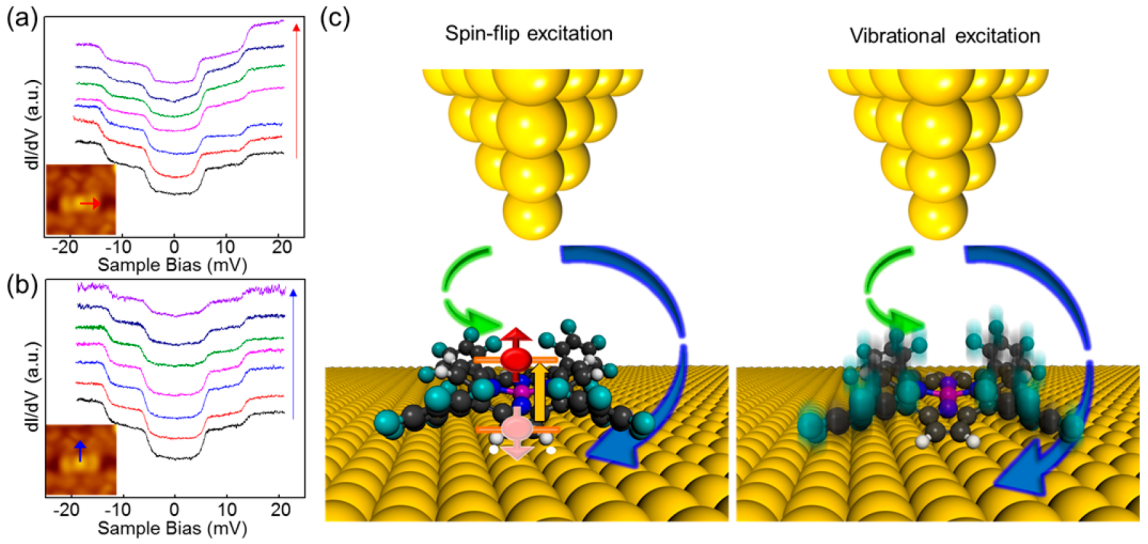

Figure 3. Spatial distribution of dI/dV signal at 0.4 K. (a) Sequence of dI/dV signals recorded along red arrow at 0.4 K and zero magnetic field and (b) sequence of dI/dV signals recorded along blue arrow at 0.4 K and zero magnetic field marked in Figure 2a. (U = −20 mV, I = 0.3 nA; V_{rms} = 0.5 mV). The spectra from bottom to top are measured from the center toward the edge and are vertically displaced for clarity. (c) Schematic images showing the spin-flip excitation and vibrational excitation.

1b), similar to that of CoTPP/Ag(111)[17,18] and FeTPP/Au(111).[11,19] The electronic properties of FeF_{20}TPP molecules are characterized by measuring site-specific dI/dV spectra at three locations along the molecular mirror-symmetry axis for each azimuthal orientation at 4.2 K. The dI/dV spectra of the molecules with different azimuthal orientation are almost identical (Figure 1c,d). All dI/dV spectra show similar features. We assign the peaks at −0.9 and 1.3 V to the highest occupied molecular orbital (HOMO) and the lowest unoccupied molecular orbital (LUMO), respectively. The dI/dV maps taken at −0.9 and 1.3 V illustrate the spatial distribution of the HOMO and LUMO, respectively, as seen in Figure 1e,f. The electronic structures of the FeF_{20}TPPmolecules on Au(111) are very similar to that of the unfluorinated FeTPP on Au(111).[11]

To clarify the physical origin of the dip feature at E_F, we measured a series of tunneling spectra along the molecular mirror-symmetry axes (the red and blue lines in Figure 2a) at 4.2 K, which are plotted in Figure 2c,d. Despite the variation of the intensity and line shape, all spectra show a similar pronounced dip feature at E_F. The dI/dV map of FeF_{20}TPP at zero bias (Figure 2b) shows an intramolecular distribution of the dip feature. Similar zero-bias dips in dI/dV spectra collected from magnetic molecules adsorbed on metal surfaces, for example, TBrPP-Co/Cu(111),[3−5] FeTPyP/Au(111),[10] and FeTPP/Au(111),[11] have been reported in the literature. In these reports such dips were interpreted as Kondo antiresonance. The intramolecular distribution of the dips was attributed to a spatially extended Kondo state in the molecules induced by interfacial charge transfer.[5,11] Assuming that the pronounced dip in our dI/dV spectra originates from a Kondo effect, T_k deduced by fitting the dips with a Fano function is in the range of 120−150 K. This unusually high T_k is in line with previous reports.[3−11]

To suppress the thermal broadening and improve the energy resolution, we acquired the dI/dV spectra at 0.4 K. Astonishingly different from the pronounced zero-bias dip at 4.2 K (Figure 2e), the dI/dV spectra taken at 0.4 K exhibit three pairs of steps around E_F, as shown in Figure 2f. These steps are symmetric with respect to E_F, indicating an origin related to inelastic electron tunneling processes.[2,20−22] These experiments show that the pronounced zero-bias dip at 4.2 K cannot be attributed to a Kondo antiresonance but has to be due to thermal broadening of steps that are due to the opening of inelastic tunneling channels as a consequence of molecular excitation.

To determine the nature of the feature shown in Figure 2f, spectra were acquired on the molecular skeleton along two paths at 0.4 K, as shown in Figure 3a,b. All spectra along the two paths exhibit pairs of steps symmetric with respect to E_F, similar to the spectra acquired at the central Fe^{2+} ion, despite the variation of the intensity. Therefore, the pronounced zero-bias dips in the spectra acquired on the molecular skeleton at 4.2 K are also not due to Kondo resonances but are due to inelastic electron tunneling (IET).

It is known that the low-lying step-like increase in dI/dV could be due to both spin-flip[21,22] and vibrational excitations[23,24] (Figure 3c). To resolve the question of the origin of the inelastic features, we measured the dI/dV spectra on the central Fe^{2+} ion (Figure S4) and on the molecular skeleton (Figure S5) with an applied magnetic field perpendicular to the Au(111) surface (B_z) at 0.4 K. The steps in the dI/dV spectra do not shift in a systematic manner with increasing B_z (Figure S4), which excludes a spin-related origin. In addition, the spatial distribution of inelastic electron tunneling spectroscopy (IETS) is inconsistent with the fact that the magnetic moment is essentially localized on the central Fe^{2+} ion (Figure S3).[25]

Conversely, the spatial distribution is well explained if the features are related to vibrational excitations, because the low-lying vibrational modes are most likely related to delocalized oscillations. Localized oscillations are typically in the high-energy regime as they depend more strongly on the deformation of intramolecular bonds and, because the coupling amplitude for vibrational excitations is inversely proportional to the excitation energy, they play a negligible role in this system. The low-energy vibrational modes of the in situ molecule are modeled using density functional theory (DFT) by solving the dynamical matrix for ionic motion of each constituent atom in the presence of a static gold substrate. We find several modes

DOI: 10.1021/acs.nanolett.7b01963
Nano Lett. 2017, 17, 4929−4933

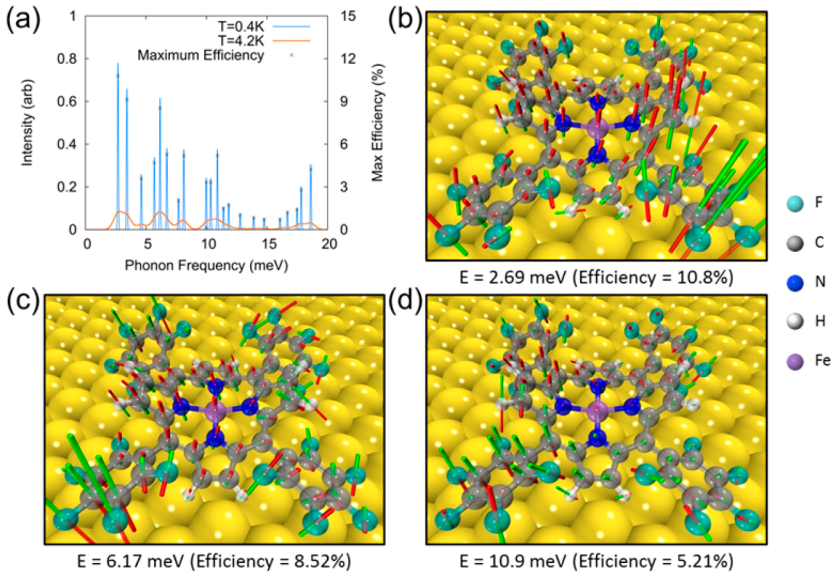

Figure 4. Spatial distribution of IETS at 0.4 K. (a) Simulated IES, showing a number of low-lying vibrational modes in the range below 20 meV. The quantum efficiencies are then defined as the ratio of the total change in conductance and the unperturbed elastic conductance. (b–d) The oscillations for the most efficient phonon modes in the region for the first and second peak of the experimental IETS. The movement of each ion is represented by vectors (green/red) given the direction of the oscillation (positive/negative).

below 20 meV each associated with an oscillation that is spatially extended over the entire molecule (see Figure 4a). Each of these modes has a different quantum efficiency, which is a measure of the strength of the electron–phonon coupling.[26−28] It can be expected that the steplike change of conductance observed at 6 and 12 meV is due to a convolution of distinct modes (see Figure 4a). We found a number of vibrational modes with high quantum efficiencies around 3–8 meV and around 10–15 meV. As a case in point, Figure 4b–d shows three of these modes, which are extended throughout the molecule, in line with experiments. The interpretation of the spectra as originating from vibrational modes is supported by the fact that the energies of the steps remain unchanged as the tip is moved from the center to the outer edge of the molecule (Figure 3a,b) and the fact that the step energies are not strongly affected by applied magnetic fields (Figure S4).

In summary, we have shown experimental spectra and corresponding theoretical simulations of $FeF_{20}TPP$ molecules adsorbed on Au(111) at both 4.2 and 0.4 K. A zero-bias dip is observed at 4.2 K, which initially appears to be due to a Kondo antiresonance, which is a common interpretation in the literature. However, as extensive experimental and theoretical analysis reveals, the feature is due to ultralow-energy vibrational excitations of the whole molecular frame. In molecular bilayer systems, these ultralow-energy vibrations can easily be excited under ambient conditions, which may contribute to the very high quantum efficiency of electron hole separation in photosynthesis.

Methods. The experiments were carried out in an ultrahigh vacuum (base pressure of 1×10^{-10} mbar) LT-STM system (Unisoku) equipped with standard surface processing facilities. Low temperature of 0.4 K is achieved by means of a single-shot ^{3}He cryostat. A magnetic field up to 11 T can be applied perpendicularly to the sample surface. An atomically flat Au(111) surface was prepared by repeated cycles of sputtering with argon ions and annealing at 800 K. The $FeF_{20}TPPCl$ molecules were deposited onto the Au(111) surface at room temperature. The sample was then transferred into the LT-STM head and cooled down. STM images were acquired in the constant-current mode. dI/dV spectra were collected by using a lock-in technique with a sinusoidal modulation at a frequency of 973.1 Hz. All STM/STS experiments were performed with electrochemically etched tungsten tips, which were calibrated against the well-known surface state of the Au(111) surface before and after spectroscopic measurements.

All DFT calculations were performed with the Vienna ab initio simulation package (VASP) and the projector augmented wave (PAW) method.[29,30] Exchange and correlation potential were described by the Perdew–Burke–Ernzerhof functional extended to incorporate a van der Waals correction.[31−33] The periodic slab model of the metal substrate includes four Au layers and a vacuum layer with a thickness of 15 Å. In-plane size of the cell is 23 Å × 20 Å. In geometric optimizations, the bottom Au layer was fixed, while the other Au layers and the molecule were fully relaxed until the residual forces were smaller than 0.02 eV/Å. Only the Γ-point in Brillouin zone is used for structural optimization and the calculation of the dynamical matrix. In order to calculate the dynamical matrix, the Au substrate ions were fixed and the constituent ions of the molecule were individually moved through all degrees of freedom to find the associated spring constant. The phonon frequencies are evaluated from the eigenvalues of the dynamical matrix and the oscillations from the eigenvectors.

■ ASSOCIATED CONTENT

Supporting Information

The Supporting Information is available free of charge on the ACS Publications website at DOI: 10.1021/acs.nanolett.7b01963.

Additional information on the on-surface dechlorination reactions of $FeF_{20}TPPCl$ and self-assembly of $FeF_{20}TPP$, molecular orbitals of $FeF_{20}TPP$ with different azimuthal orientation on Au(111), IETS taken on central Fe^{2+} ion with increasing magnetic field and on the molecular frame with increasing magnetic field at 0.4 K (PDF)

DOI: 10.1021/acs.nanolett.7b01963
Nano Lett. 2017, 17, 4929–4933

AUTHOR INFORMATION

Corresponding Authors

*E-mail: hjgao@iphy.ac.cn.
*E-mail: sxdu@iphy.ac.cn.
*E-mail: Werner.Hofer@newcastle.ac.uk.

ORCID

Jun-Long Zhang: 0000-0002-5731-7354
Yu-Yang Zhang: 0000-0002-9548-0021
Shixuan Du: 0000-0001-9323-1307
Hong-Jun Gao: 0000-0002-6766-0623

Author Contributions

⊥H.C., T.P, Z.W, and D.W. contributed equally to this work.

Notes

The authors declare no competing financial interest.

ACKNOWLEDGMENTS

This work was supported by grants from the National Science Foundation of China (51210003, 61574170, 51325204), National "973" projects of China (2013CBA01601, 2015CB921103), the Chinese Academy of Sciences, and the CAS Pioneer Hundred Talents Program. Work at Vanderbilt (S.T.P. and Y.Y.Z.) was supported by the U.S. Department of Energy through Grant DE-FG02-09ER46554 and the McMinn Endowment. Y.Y.Z and S.T.P acknowledge the National Energy Research Scientific Computing Center (NERSC), a DOE Office of Science User Facility supported by the Office of Science of the U.S. Department of Energy under Contract No. DE-AC02-05CH11231, and the Extreme Science and Engineering Discovery Environment (XSEDE), which is supported by National Science Foundation Grant ACI-1053575. W.A.H. acknowledges support for the UKCP consortium, EPSRC Grant EP/K013610/1.

REFERENCES

(1) Scholes, G. D.; Fleming, G. R.; Olaya-Castro, A.; van Grondelle, R. *Nat. Chem.* **2011**, *3* (10), 763−774.
(2) Stipe, B. C.; Rezaei, M. A.; Ho, W. *Science* **1998**, *280* (5370), 1732−1735.
(3) Iancu, V.; Deshpande, A.; Hla, S. W. *Phys. Rev. Lett.* **2006**, *97* (26), 266603.
(4) Iancu, V.; Deshpande, A.; Hla, S. W. *Nano Lett.* **2006**, *6* (4), 820−823.
(5) Perera, U. G.; Kulik, H. J.; Iancu, V.; Dias da Silva, L. G.; Ulloa, S. E.; Marzari, N.; Hla, S. W. *Phys. Rev. Lett.* **2010**, *105* (10), 106601.
(6) Dilullo, A.; Chang, S. H.; Baadji, N.; Clark, K.; Klockner, J. P.; Prosenc, M. H.; Sanvito, S.; Wiesendanger, R.; Hoffmann, G.; Hla, S. W. *Nano Lett.* **2012**, *12* (6), 3174−3179.
(7) Wu, F.; Liu, J.; Mishra, P.; Komeda, T.; Mack, J.; Chang, Y.; Kobayashi, N.; Shen, Z. *Nat. Commun.* **2015**, *6*, 7547.
(8) Gopakumar, T. G.; Matino, F.; Naggert, H.; Bannwarth, A.; Tuczek, F.; Berndt, R. *Angew. Chem., Int. Ed.* **2012**, *51* (25), 6262−6266.
(9) Heinrich, B. W.; Ahmadi, G.; Muller, V. L.; Braun, L.; Pascual, J. I.; Franke, K. J. *Nano Lett.* **2013**, *13* (10), 4840−4843.
(10) Lin, T.; Kuang, G.; Wang, W.; Lin, N. *ACS Nano* **2014**, *8* (8), 8310−8316.
(11) Wang, W.; Pang, R.; Kuang, G.; Shi, X.; Shang, X.; Liu, P. N.; Lin, N. *Phys. Rev. B: Condens. Matter Mater. Phys.* **2015**, *91* (4), 045440.
(12) Madhavan, V.; Chen, W.; Jamneala, T.; Crommie, M. F.; Wingreen, N. S. *Science* **1998**, *280* (5363), 567−569.
(13) Manoharan, H. C.; Lutz, C. P.; Eigler, D. M. *Nature* **2000**, *403* (6769), 512−515.
(14) Knorr, N.; Schneider, M. A.; Diekhoner, L.; Wahl, P.; Kern, K. *Phys. Rev. Lett.* **2002**, *88* (9), 096804.
(15) Wahl, P.; Diekhoner, L.; Schneider, M. A.; Vitali, L.; Wittich, G.; Kern, K. *Phys. Rev. Lett.* **2004**, *93* (17), 176603.
(16) Liang, L.; Lv, H. B.; Yu, Y.; Wang, P.; Zhang, J. L. *Dalton Trans.* **2012**, *41* (5), 1457−1460.
(17) Hieringer, W.; Flechtner, K.; Kretschmann, A.; Seufert, K.; Auwarter, W.; Barth, J. V.; Gorling, A.; Steinruck, H. P.; Gottfried, J. M. *J. Am. Chem. Soc.* **2011**, *133* (16), 6206−6222.
(18) Seufert, K.; Auwarter, W.; Barth, J. V. *J. Am. Chem. Soc.* **2010**, *132* (51), 18141−18146.
(19) Gopakumar, T. G.; Tang, H.; Morillo, J.; Berndt, R. *J. Am. Chem. Soc.* **2012**, *134* (29), 11844−11847.
(20) Yu, A.; Li, S.; Czap, G.; Ho, W. *J. Phys. Chem. C* **2015**, *119* (26), 14737−14741.
(21) Heinrich, A. J.; Gupta, J. A.; Lutz, C. P.; Eigler, D. M. *Science* **2004**, *306* (5695), 466−469.
(22) Hirjibehedin, C. F.; Lin, C. Y.; Otte, A. F.; Ternes, M.; Lutz, C. P.; Jones, B. A.; Heinrich, A. J. *Science* **2007**, *317* (5842), 1199−1203.
(23) Hofer, W. A.; Teobaldi, G.; Lorente, N. *Nanotechnology* **2008**, *19* (30), 305701.
(24) Pivetta, M.; Ternes, M.; Patthey, F.; Schneider, W. D. *Phys. Rev. Lett.* **2007**, *99* (12), 126104.
(25) Tsukahara, N.; Noto, K.; Ohara, M.; Shiraki, S.; Takagi, N.; Takata, Y.; Miyawaki, J.; Taguchi, M.; Chainani, A.; Shin, S.; Kawai, M. *Phys. Rev. Lett.* **2009**, *102* (16), 167203.
(26) Teobaldi, G.; Penalba, M.; Arnau, A.; Lorente, N.; Hofer, W. A. *Phys. Rev. B: Condens. Matter Mater. Phys.* **2007**, *76* (23), 235407.
(27) Lorente, N. *Appl. Phys. A: Mater. Sci. Process.* **2004**, *78* (6), 799−806.
(28) Ulusoy, I. S.; Scribano, Y.; Benoit, D. M.; Tschetschetkin, A.; Maurer, N.; Koslowski, B.; Ziemann, P. *Phys. Chem. Chem. Phys.* **2011**, *13* (2), 612−618.
(29) Vanderbilt, D. *Phys. Rev. B: Condens. Matter Mater. Phys.* **1990**, *41* (11), 7892−7895.
(30) Kresse, G.; Furthmuller, J. *Phys. Rev. B: Condens. Matter Mater. Phys.* **1996**, *54* (16), 11169.
(31) Grimme, S. *J. Comput. Chem.* **2006**, *27* (15), 1787−1799.
(32) Lee, K.; Murray, E. D.; Kong, L. Z.; Lundqvist, B. I.; Langreth, D. C. *Phys. Rev. B: Condens. Matter Mater. Phys.* **2010**, *82* (8), 081101.
(33) Dion, M.; Rydberg, H.; Schroder, E.; Langreth, D. C.; Lundqvist, B. I. *Phys. Rev. Lett.* **2004**, *92* (24), 246401.

DOI: 10.1021/acs.nanolett.7b01963
Nano Lett. 2017, 17, 4929−4933